

Tensor-product vertex patch smoothers for biharmonic problems

Julius Witte* Cu Cui*[†] Francesca Bonizzoni[‡]
 Guido Kanschat*[§]

December 9, 2024

Abstract

We discuss vertex patch smoothers as overlapping domain decomposition methods for fourth order elliptic partial differential equations. We show that they are numerically very efficient and yield high convergence rates. Furthermore, we discuss low rank tensor approximations for their efficient implementation. Our experiments demonstrate that the inexact local solver yields a method which converges fast and uniformly with respect to mesh refinement. The multiplicative smoother shows superior performance in terms of solution efficiency, requiring fewer iterations. However, in three-dimensional cases, the additive smoother outperforms its multiplicative counterpart due to the latter’s lower potential for parallelism. Additionally, the solver infrastructure supports a mixed-precision approach, executing the multigrid preconditioner in single precision while performing the outer iteration in double precision, thereby increasing throughput by up to 70%.

1 Introduction

Recent years have seen a major adaptation of finite element software to modern hardware with its high levels of parallelism and an increasing gap between computing and memory speed. The key to this progress is high computational intensity. In this article, we address this issue by proposing a highly optimized

*Interdisciplinary Center for Scientific Computing (IWR), Heidelberg University, Im Neuenheimer Feld 205, 69120 Heidelberg, Germany

[†]Supported by the China Scholarship Council (CSC) under grant no. 202106380059

[‡]MOX, Department of Mathematics, Politecnico di Milano, Piazza Leonardo da Vinci 32, 20133 Milano, Italy. FB has received support from the project PRIN2022, MUR, Italy, 2023–2025, P2022N5ZNP “SIDDMs: shape-informed data-driven models for parametrized PDEs, with application to computational cardiology”. FB is partially funded by “INdAM - GNCS Project”, codice CUP E53C23001670001. FB is member of INdAM-GNCS

[§]Supported by the Deutsche Forschungsgemeinschaft (DFG) under Germany’s Excellence Strategy EXC 2181/1 - 390900948 (the Heidelberg STRUCTURES Excellence Cluster)

multigrid smoother for the biharmonic problem and its implementation on a recent GPU accelerator.

The standard for efficient implementation of finite element methods has improved considerably in recent years [KK12, KK19, MGS01] by the shift from sparse matrices to a computation of the action of the bilinear form to a vector on the fly. The amount of memory transfers was reduced considerably at the cost of additional computations on the data vector. Using sum factorization, the additional cost could be kept in check and the speed-up for applying the finite element operator to a vector was significant. The development on the side of solvers was lagging behind for some time, as multigrid smoothers did either not provide the same computational intensity measured in floating point operations per byte loaded from main memory, or were very expensive.

In order to solve the biharmonic problem, we focus on an implementation of the C^0 interior penalty method (C0IP) of [BS05] albeit there is preceding work on multigrid for the biharmonic problem in [Zha89, Zha05]. A multigrid method for C0IP with uniform convergence was developed in [BZ05]. In [BW05] two-level additive Schwarz preconditioners with a generic overlap at the scale of fine-level elements were analyzed. Similarly, in [FK05], theory on two-level non-overlapping additive and multiplicative Schwarz smoothers was provided, proving a bound for the condition number of $\mathcal{O}(H^3/h^3)$. The same bounds were demonstrated for isogeometric discretizations in [CPS18].

These works mainly focused on mathematical efficiency and did not address the question computational efficiency. To this end, we combine overlapping domain decomposition methods with multigrid. In order to have efficient local solvers, we choose vertex patches as subdomains, since on quadrilateral and hexahedral meshes they have tensor product structure. By [KS14], we can directly relate to our recent work on Stokes equations [CK24a]. The key technique is the fast diagonalization method (FDM) from [LRT64], which we apply in an approximate fashion as the local operators do not admit a rank two tensor representation.

Previous works [CGBKS24, CK24b] have demonstrated the efficient implementation of vertex-patch smoothers on GPUs using the Poisson problem as a test case. By leveraging efficient shared memory utilization and optimized memory access patterns, these implementations achieved performance close to the shared memory roofline limits for most polynomial degrees. For instance, on an NVIDIA A100 GPU, the FP64 performance of vertex-patch smoothers and matrix-vector product kernels exceeded 3 TFLOPS, reaching 36% of the theoretical peak performance, with similar efficiency observed for FP32. This approach was subsequently extended to solve the Stokes problem [CK24a]. Building on these advancements and taking advantage of the separable representation of the local solvers in the smoothers proposed in this work and its efficient evaluation with the fast diagonalization method, we follow the same implementation strategy to address biharmonic problems in this study.

In the following section, we introduce the model problem and its discretization. Section 3 describes the multigrid method and the additive and multiplicative vertex patch smoothers. In Section 4, we discuss the tensor structure of

the local problems which allows us to apply a fast approximate local solver. We present experimental results for various aspects of the method in Section 5 before concluding.

2 Model problem and discretization

In this article, we discuss a method for the model problem of the biharmonic equation

$$\begin{aligned} -\Delta^2 u &= f && \text{in } \Omega, \\ u &= 0 && \text{on } \partial\Omega, \\ \nabla u \cdot \mathbf{n} &= 0 && \text{on } \partial\Omega, \end{aligned} \tag{1}$$

where Ω is a polygonal domain in \mathbb{R}^d with $d = 2, 3$. The volumetric load f is a given data. The boundary conditions are referred to as clamped. The natural (weak) solution space for the biharmonic equation with clamped boundary conditions is $H_0^2(\Omega)$. The C^0 -continuity and vanishing traces at the physical boundary already implies that the tangential derivative vanishes as well at $\partial\Omega$. Then, the weak problem reads: find $u \in H_0^2(\Omega)$ such that

$$a(u, v) = F(v) \quad \forall v \in H_0^2(\Omega), \tag{2}$$

where

$$a(u, v) = \int_{\Omega} \nabla^2 u : \nabla^2 v \, d\mathbf{x}, \quad F(v) = \int_{\Omega} f v \, d\mathbf{x}. \tag{3}$$

Here, the second order tensor $\nabla^2 v$ denotes the Hessian matrix of a scalar field v and the Hadamard product $A : B$ denotes the full contraction of second order tensors A and B .

Note that $a(u, u)$ is the square of the L^2 -norm of the function $\nabla^2 u$. Applying Friedrichs' inequality twice, it thus introduces an inner product on $H_0^2(\Omega)$. Hence, the weak formulation (2) is well-posed.

The C^0 interior penalty method (COIP) was introduced by Brenner and Sung [BS05, Bre11] as a convenient discretization scheme for fourth order equations based on continuous finite element methods and a penalization of discontinuous first derivative by terms in the fashion of interior penalty methods [Arn82, Nit71].

We choose standard Lagrange finite elements on quadrilaterals and hexahedra with shape function spaces \mathbb{Q}_k consisting of (mapped) tensor product polynomials of degree k . Moreover, in order to prepare for multigrid methods, we discretize the domain Ω by a nested sequence of meshes

$$\mathbb{T}_0 \sqsubset \mathbb{T}_1 \sqsubset \cdots \sqsubset \mathbb{T}_\ell \sqsubset \cdots \sqsubset \mathbb{T}_L,$$

consisting of quadrilaterals or hexahedra of size h_ℓ . While our results are obtained on Cartesian meshes, the discretization only requires shape regular, locally uniform cells. The relation “ \sqsubset ” indicates that all cells of a mesh \mathbb{T}_ℓ are obtained by refinement of the cells of $\mathbb{T}_{\ell-1}$. Refinement is obtained by dividing

all edges of a cell in two and reconnecting in the natural way to 2^d new cells. On these meshes, we define finite element spaces V_ℓ by

$$V_\ell = \left\{ v \in H_0^1(\Omega) \mid v|_K \in \mathbb{Q}_k \quad \forall K \in \mathbb{T}_\ell \right\}. \quad (4)$$

From the definition it becomes apparent that V_ℓ is non-conforming, that is, V_ℓ is not a subspace of $H_0^2(\Omega)$. Therefore, we follow [BS05] and introduce interface terms penalizing jumps in the derivative.

Let \mathbb{E}_ℓ° and \mathbb{E}_ℓ^∂ denote the set of interior and boundary facets of \mathbb{T}_ℓ , respectively, and let $\mathbb{E}_\ell = \mathbb{E}_\ell^\circ \cup \mathbb{E}_\ell^\partial$. For an interior facet e , let K^+ and K^- be the mesh cells such that $e = K^+ \cap K^-$. On e , let v^+ and v^- be the trace of a finite element function v from these cells. Let $\partial_{n^+} v^+$ and $\partial_{n^-} v^-$ be the corresponding normal derivatives. Then, we define for $\mathbf{x} \in e$ the jump of the normal derivative and the mean of the second derivative in normal direction as

$$\begin{aligned} \llbracket \partial_n v \rrbracket(\mathbf{x}) &= \partial_{n^+} v^+(\mathbf{x}) + \partial_{n^-} v^-(\mathbf{x}), \\ \left\{ \partial_n^2 v \right\}(\mathbf{x}) &= \frac{1}{2} \left(\partial_{n^+}^2 v^+(\mathbf{x}) + \partial_{n^-}^2 v^-(\mathbf{x}) \right). \end{aligned} \quad (5)$$

We emphasize that both definitions are independent of the choice of K^+ and K^- . On a boundary facet, let

$$\llbracket \partial_n v \rrbracket(\mathbf{x}) = \partial_n v(\mathbf{x}), \quad \left\{ \partial_n^2 v \right\}(\mathbf{x}) = \partial_n^2 v(\mathbf{x}). \quad (6)$$

By multiplying (1) with a test function, integration by parts, and stabilizing by Nitsche's idea, the C^0 interior penalty (C^0 -IP) formulation reads: find $u_\ell \in V_\ell$ such that

$$a_\ell(u_\ell, v_\ell) = F(v_\ell) \quad \forall v_\ell \in V_\ell \quad (7)$$

with the bilinear form

$$\begin{aligned} a_\ell(u, v) &:= \sum_{K \in \mathbb{T}_\ell} \int_K \nabla^2 u : \nabla^2 v \, d\mathbf{x} \\ &+ \sum_{e \in \mathbb{E}_\ell} \int_e \left(\frac{\gamma}{h_e} \llbracket \partial_n u \rrbracket \llbracket \partial_n v \rrbracket - \left\{ \partial_n^2 u \right\} \llbracket \partial_n v \rrbracket - \llbracket \partial_n u \rrbracket \left\{ \partial_n^2 v \right\} \right) d\sigma \end{aligned} \quad (8)$$

and the linear form F being defined in (3). We refer to the cell integral of bilinear form (8) as *bulk* term and to the three face integrals, from left to right, as *penalty*, *consistency* and *adjoint consistency* term.

We assume that the penalty parameter γ only depends on the polynomial degree k and h_e is the harmonic mean of the extent of the two mesh cells adjacent to e orthogonal to e .

We recall the following results from [Bre11, BS05]

Proposition 2.1 (Well-posedness). *Assume that γ is chosen sufficiently large. Then, the bilinear form $a_\ell(\cdot, \cdot)$ is coercive with respect to the mesh-dependent norm*

$$\|v\|_h^2 = \sum_{K \in \mathbb{T}_\ell} |v|_{2,K}^2 + \sum_{e \in \mathbb{E}_\ell} \frac{\gamma_e}{h_e} \|\llbracket \partial_n v \rrbracket\|_e^2, \quad (9)$$

on V_ℓ . Hence, (7) has a unique solution.

Furthermore, if the weak solution u to (2) belongs to $H^{k+1}(\Omega)$, then the interior penalty solution u_ℓ in (7) satisfies the energy error estimate

$$|u - u_\ell|_\ell \leq Ch_\ell^{k-1} |u|_{k+1, \Omega}. \quad (10)$$

3 Multigrid and vertex-patch smoothers

The generic structure of a single V -Cycle multigrid step is summarized in Algorithm 1. Note that pre- and post-smoothing can be one or more steps of the smoothers described below. The matrices A_ℓ are obtained from the bilinear form in equation (8) by choosing a basis for the finite element spaces V_ℓ in the standard way. The choice of tensor product basis functions will be detailed in Section 4. The prolongation $I_{\ell-1}^\uparrow: V_{\ell-1} \rightarrow V_\ell$ is the matrix of the standard

Algorithm 1 V -Cycle on level ℓ

```

1: procedure  $\text{MG}_\ell(x_\ell, b_\ell)$ 
2:   if  $\ell = 0$  then
3:      $x_0 \leftarrow A_0^{-1} b_0$  ▷ coarse grid solver
4:   end if
5:    $x_\ell \leftarrow S_\ell(x_\ell, b_\ell)$  ▷ pre-smoothing
6:    $b_{\ell-1} \leftarrow I_{\ell-1}^\downarrow (b_\ell - A_\ell x_\ell)$  ▷ restriction
7:    $e_{\ell-1} \leftarrow \text{MG}_{\ell-1}(0, b_{\ell-1})$  ▷ recursion
8:    $x_\ell \leftarrow x_\ell + I_{\ell-1}^\uparrow e_{\ell-1}$  ▷ prolongation
9:    $x_\ell \leftarrow S_\ell(x_\ell, b_\ell)$  ▷ post-smoothing
10:  return  $x_\ell$ 
11: end procedure

```

embedding operator and the restriction $I_{\ell-1}^\downarrow$ is its transpose.

The smoother is an overlapping domain decomposition method based on the multigrid method developed in [AFW97]. It is based on local solvers which solve the discretized differential equation on subdomains $\Omega_{\mathcal{V}}$ consisting of all cells attached to a vertex \mathcal{V} , so-called vertex patches, see also Figure 1. By traversing all internal vertices of the mesh, the union of the patches covers the whole domain. This method has been applied successfully to Stokes and Brinkman equations [KM15, KLM17] and it was shown that its application to the COIP method is equivalent to the Stokes equations [KS14].

To be more precise, let \mathcal{V} be an interior vertex of \mathbb{T}_ℓ and $\Omega_{\mathcal{V}}$ be its vertex patch, i. e. the union of all cells adjacent to this vertex. Then, the associated subspace $V_{\mathcal{V}} \subset V_\ell$ consists of all finite element functions with support in $\Omega_{\mathcal{V}}$. Here, we use the index ℓ for global vectors and omit it for local spaces and operators to keep the notation simple. Let $R_{\mathcal{V}}$ be the localization operator, which selects out of a coefficient vector representing a finite element function in V_ℓ only those coefficients corresponding to functions in $V_{\mathcal{V}}$. Let furthermore $A_{\mathcal{V}}$

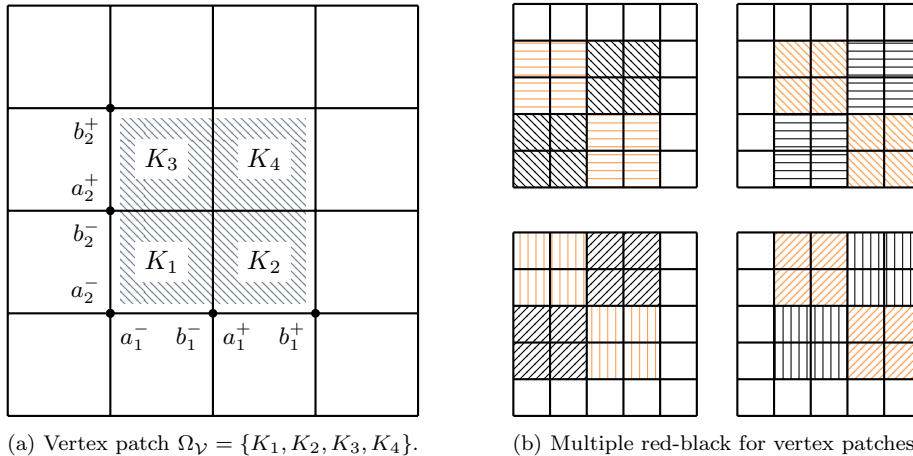


Figure 1: A Cartesian vertex patch $\Omega_{\mathcal{V}} = \{K_1, K_2, K_3, K_4\}$ consisting of four cells in two dimensions (*left*) and the coloring scheme (*right*). The hatched and dotted areas on the right-hand shows a multiple red-black coloring satisfying A_ℓ -orthogonality.

be the restriction of the matrix A_ℓ to $V_{\mathcal{V}}$. Later, we will also replace its inverse $A_{\mathcal{V}}^{-1}$ by an approximation. Then, we define the additive vertex patch smoother (AVS) as

$$S_{\ell;A}(x_\ell, b_\ell) = x_\ell - \left[\sum_{\mathcal{V}} \omega R_{\mathcal{V}}^T A_{\mathcal{V}}^{-1} R_{\mathcal{V}} \right] [b_\ell - A_\ell x_\ell], \quad (11)$$

where ω is a damping factor not exceeding the maximal number of patches overlapping in one cell, on uniform meshes $1/4$ in two and $1/8$ in three dimensions. We will also provide examples, where the AVS is applied twice. Alternatively, we define the multiplicative vertex patch smoother (MVS). To this end, we define a numbering of the vertices $\mathcal{V}_1, \dots, \mathcal{V}_J$ and recursively

$$\begin{aligned} x_\ell^{(0)} &= x_\ell, \\ \nu = 1, \dots, J: \quad x_\ell^{(\nu)} &= x_\ell^{(\nu-1)} - \omega R_{\mathcal{V}_\nu}^T A_{\mathcal{V}_\nu}^{-1} R_{\mathcal{V}_\nu} [b_\ell - A_\ell x_\ell^{(\nu-1)}], \\ S_{\ell;M}(x_\ell, b_\ell) &= x_\ell^{(J)}. \end{aligned} \quad (12)$$

This algorithm, while not suffering from the necessity to choose a small damping factor, has two drawbacks. It is inherently sequential and there is a product with the matrix A_ℓ in every substep. The latter can be fixed for instance by using local residual computations as in [WMKK24]. We fix both issues by so-called coloring. This technique is inspired by the well-known red-black Gauss-Seidel method. First, we note that we obviously cannot write data of the same cell in a concurring way. Hence, in a first step, we split the set of all vertex patches

into subsets of nonoverlapping patches called “colors”, see the four meshes in Figure 1 on the right. The computed update of each local vertex patch solver only affects the solution inside the patch. Hence, these updates can be written at once and in parallel without fearing race conditions. But since the discontinuous Galerkin method reads from neighboring patches, we have to rely on that data to remain unchanged. This is achieved by the red-black coloring inside each nonoverlapping subset. Hence, on a uniform mesh, we obtain 8 colors in two and 16 colors in three dimensions. Applying this scheme to the multiplicative algorithm with n_c colors, and \mathbb{V}_i being the set of all patches in color i , we obtain the following method:

$$\begin{aligned}
x_\ell^{(0)} &= x_\ell \\
\nu = 1, \dots, n_c: \quad x_\ell^{(\nu)} &= x_\ell^{(\nu-1)} - \left[\sum_{\mathcal{V} \in \mathbb{V}_\nu} \omega R_{\mathcal{V}_\nu}^T A_{\mathcal{V}_\nu}^{-1} R_{\mathcal{V}_\nu} \right] [b_\ell - A_\ell x_\ell^{(\nu-1)}], \quad (13) \\
S_{\ell;M}(x_\ell, b_\ell) &= x_\ell^{(n_c)}
\end{aligned}$$

Since the summations are nonoverlapping, we do not have the strict restriction on the damping factor ω . Furthermore, we only have n_c global operator applications instead of J . Finally, all the local solvers inside the sum can be applied in parallel. Hence, this is the implementation of the multiplicative smoother we use in the experiments.

4 Tensor structure

In this section we aim at highlighting the tensor product structure of the C^0 -IP bilinear form (8), when restricted to a regular vertex patch. To this end, let us take rank-two trial and test functions φ_j, φ_i of the form

$$\begin{aligned}
\varphi_j(x_1, x_2) &= \phi_{j_1}(x_1)\phi_{j_2}(x_2), \\
\varphi_i(x_1, x_2) &= \phi_{i_1}(x_1)\phi_{i_2}(x_2),
\end{aligned} \quad (14)$$

where $\mathbf{i} = (i_1, i_2)$ and $\mathbf{j} = (j_1, j_2)$, and let us focus on the vertex patch $\Omega_{\mathcal{V}} := \{K_1, K_2, K_3, K_4\}$ represented in Figure 1 (left). Inserting φ_j, φ_i into (8) restricted to \mathcal{V}_K , we get

$$\sum_{K \in \Omega_{\mathcal{V}}} \int_K \nabla^2 \varphi_j : \nabla^2 \varphi_i \, d\mathbf{x} + \quad (15)$$

$$\sum_{K \in \Omega_{\mathcal{V}}} \sum_{e \in \partial K} \int_e \left(\frac{\gamma}{h_e} \llbracket \partial_n \varphi_j \rrbracket \llbracket \partial_n \varphi_i \rrbracket - \left\{ \partial_n^2 \varphi_j \right\} \llbracket \partial_n \varphi_i \rrbracket - \llbracket \partial_n \varphi_j \rrbracket \left\{ \partial_n^2 \varphi_i \right\} \right) d\sigma. \quad (16)$$

Exploiting the tensor product form (14) of the test and trial function, we can explicitly write the bulk term (15) as follows

$$(15) = \left[\int_{a_1^-}^{b_1^-} \phi_{j_1}'' \phi_{i_1}'' dx_1 + \int_{a_1^+}^{b_1^+} \phi_{j_1}'' \phi_{i_1}'' dx_1 \right] \int_{a_2^-}^{b_2^+} \phi_{j_2} \phi_{i_2} dx_2 \quad (17)$$

$$+ 2 \int_{a_1^-}^{b_1^+} \phi_{j_1}' \phi_{i_1}' dx_1 \int_{a_2^-}^{b_2^+} \phi_{j_2}' \phi_{i_2}' dx_2 \quad (18)$$

$$+ \int_{a_1^-}^{b_1^+} \phi_{j_1} \phi_{i_1} dx_1 \left[\int_{a_2^-}^{b_2^-} \phi_{j_2}'' \phi_{i_2}'' dx_2 + \int_{a_2^+}^{b_2^+} \phi_{j_2}'' \phi_{i_2}'' dx_2 \right]. \quad (19)$$

Analogously, we can reformulate the expression of the face integrals (16). For instance, let e be the vertical edge $e = b_1^- \times [a_2^-, b_2^-]$, see also Figure 1 (left). Then, the face integral

$$\int_e \left(\frac{\gamma}{h_e} \llbracket \partial_n \varphi_j \rrbracket \llbracket \partial_n \varphi_i \rrbracket - \left\{ \partial_n^2 \varphi_j \right\} \llbracket \partial_n \varphi_i \rrbracket - \llbracket \partial_n \varphi_j \rrbracket \left\{ \partial_n^2 \varphi_i \right\} \right) d\sigma \quad (20)$$

becomes

$$\left(\frac{\gamma}{(|b_2^- - a_2^-|)} \llbracket \phi_{j_1}' \rrbracket \llbracket \phi_{i_1}' \rrbracket - \left\{ \phi_{j_1}'' \right\} \llbracket \phi_{i_1}' \rrbracket - \llbracket \phi_{j_1}' \rrbracket \left\{ \phi_{i_1}'' \right\} \right) \int_{a_2^-}^{b_2^-} \phi_{j_2} \phi_{i_2} dx_2. \quad (21)$$

For integrals over horizontal edges we have to swap the two dimensions. Namely, given $e = [a_1^-, b_1^-] \times b_2^-$, the face integral (20) becomes

$$\left(\frac{\gamma}{(|b_1^- - a_1^-|)} \llbracket \phi_{j_2}' \rrbracket \llbracket \phi_{i_2}' \rrbracket - \left\{ \phi_{j_2}'' \right\} \llbracket \phi_{i_2}' \rrbracket - \llbracket \phi_{j_2}' \rrbracket \left\{ \phi_{i_2}'' \right\} \right) \int_{a_1^-}^{b_1^-} \phi_{j_1} \phi_{i_1} dx_1. \quad (22)$$

As a consequence, the C^0 -IP discretization matrix for a regular vertex patch has the following rank-3 tensor representation

$$B^{(1)} \otimes M^{(2)} + 2L^{(1)} \otimes L^{(2)} + M^{(1)} \otimes B^{(2)}, \quad (23)$$

where $M^{(d)}$ and $L^{(d)}$ denote the mass and stiffness matrices along the direction d , namely,

$$M_{ij}^{(d)} = \int_{a_d^-}^{b_d^+} \phi_j \phi_i dx, \quad L_{ij}^{(d)} = \int_{a_d^-}^{b_d^+} \phi_j' \phi_i' dx, \quad (24)$$

and the matrices $B^{(d)}$ are computed from (18), (21) and (22). In three dimensions, we obtain with the same arguments

$$B^{(1)} \otimes M^{(2)} \otimes M^{(3)} + M^{(1)} \otimes B^{(2)} \otimes M^{(3)} + M^{(1)} \otimes M^{(2)} \otimes B^{(3)} \\ + 2L^{(1)} \otimes L^{(2)} \otimes M^{(3)} + 2M^{(1)} \otimes L^{(2)} \otimes L^{(3)} + 2L^{(1)} \otimes M^{(2)} \otimes L^{(3)}. \quad (25)$$

The above representation can also be utilized to perform matrix-vector multiplication. The matrix-free evaluation of the finite element operator Ax using sum factorization has a computational complexity of $\mathcal{O}(dk^{d+1})$ [KK12, KK19]. Since the finite element operator can be expressed as a sum of Kronecker products, as shown in (23) and (25), this can be viewed as a specialized optimization. This approach involves fewer sum-factorization sweeps compared to standard numerical integration. It is important to note that these separable matrices are only applicable in the case of constant coefficients and axis-aligned meshes. The parallelization of this operator is implemented in a patch-wise manner [CK24b], where partial cells and faces are processed within each patch. This approach not only avoids redundant integration computations but also improves data locality. Potential write conflicts can be avoided by so-called atomic operations.

4.1 Fast Diagonalization

Here, we develop local solvers for the smoother which have the same complexity as the matrix-vector product above. To this end, we have to use the tensor structure again. The fast diagonalization method was introduced in [LRT64] with the aim of efficiently solving second order separable partial differential equations in any dimension $d \geq 2$. For simplicity, let $d = 2$. For any operator of the form

$$A = A_1 \otimes M_2 + M_1 \otimes A_2, \quad (26)$$

its inverse can be computed as

$$A^{-1} = (Q_1 \otimes Q_2) (\Lambda_1 \otimes I_2 + I_1 \otimes \Lambda_2)^{-1} (Q_1 \otimes Q_2)^\top, \quad (27)$$

where the diagonal matrices Λ_i and the unitary matrices Q_i solve the generalized eigenvalue problems

$$Q_i^\top A_i Q_i = \Lambda_i M_i, \quad \text{for } i = 1, \dots, d.$$

Notice that in formula (27) the inverse is taken over the diagonal matrices Λ_i and the unitary matrices Q_i can be applied separately in each direction. Hence, the application of A^{-1} to a vector is indeed achieved with a complexity of $\mathcal{O}(dk^{d+1})$.

The operator (23) that represents the discretization of the biharmonic problem in $2d$ is not a rank-2 operator. Indeed, the elementary tensor $L^{(1)} \otimes L^{(2)}$ involving first order partial derivatives with respect to the first as well as second coordinate, prevents us from a separable tensor structure. A similar discussion holds in dimension $d = 3$, where the terms of (25) that destroy the separable structure are $L^{(1)} \otimes L^{(2)} \otimes M^{(3)}$, $M^{(1)} \otimes L^{(2)} \otimes L^{(3)}$, $L^{(1)} \otimes M^{(2)} \otimes L^{(3)}$. As a consequence, the exact local solvers are not amenable to fast diagonalization.

On the other hand, if we omit the terms involving mixed first order partial derivatives arising from the bulk term, the local solvers on Ω_{ν_j} become inexact but with separable representation in two and three dimensions, respectively,

$$\tilde{A}_j = B_j^{(1)} \otimes M_j^{(2)} + M_j^{(1)} \otimes B_j^{(2)}, \quad (28)$$

$$\tilde{A}_j = B_j^{(1)} \otimes M_j^{(2)} \otimes M_j^{(3)} + M_j^{(1)} \otimes B_j^{(2)} \otimes M_j^{(3)} + M_j^{(1)} \otimes M_j^{(2)} \otimes B_j^{(3)}. \quad (29)$$

Note that $B_j^{(i)}$ and $M_j^{(i)}$ are both symmetric as well as positive semi-definite or positive definite, respectively, for $i = 1, \dots, d$. Consequently, the generalized eigenvalue problems required for fast diagonalization are well-defined. Besides, positive definiteness of \tilde{A}_j ensures that the local stability assumption is satisfied.

5 Computational experiments

We have implemented the numerical algorithms described above in the framework of the finite element library deal.II [ABB⁺23]. The experiments use a system with an NVIDIA A100 GPU, hosted with two AMD EPYC 7282 16-core processors. The GPU has 80GB of high-speed HBM2e memory, providing 2TB/s peak memory bandwidth, and offers peak FP64 performance of 8.7 TFLOPS and FP32 performance of 17.4 TFLOPS on CUDA Cores and peak FP64 performance of 17.4 TFLOPS on Tensor Cores.

Building on our previous work [CGBKS24] on the Poisson problem, we will describe important practical details that were required to obtain performant implementations for these algorithms. To achieve high performance on GPUs, the most critical factor is the efficient utilization of the limited on-chip memory, commonly referred to as *Shared Memory*, which offers lower latency and higher bandwidth. Following the approach from our previous work, we leverage shared memory to perform computations, thereby avoiding random high-latency global memory accesses.

The key to effectively utilizing shared memory lies in optimizing memory access patterns. By employing the conflict-free memory access pattern developed in our earlier work, optimal performance is achieved, where all memory load or store operations within a warp are serviced simultaneously without causing any *bank conflicts*¹. This optimal access pattern has been validated using the NVIDIA Nsight Compute profiler [NVI23]. Finally, the entire solution process is performed exclusively on the GPU, eliminating data transfers between the CPU and the GPU, further enhancing performance and reducing latency.

When running a parallel for loop over all vertex patches of the additive smoother, the local operation on each patch can potentially lead to a race condition. This is because two overlapped patches will write or load the data from the same cell. Therefore, a similar colored algorithm used in the multiplicative algorithm can be applied to address this issue (referred to as *colored AVS*). In this work, we also consider an alternative approach that leverages atomic operations to address this issue. On modern GPUs, atomic operations are executed with a single instruction using a “fire-and-forget” semantic. This means that the instruction returns immediately, with conflict resolution managed by the cache system. Furthermore, modern GPUs provide support for fast atomic operations on double precision values. We denote this approach by *atomic AVS*.

¹Shared memory is organized into multiple equally sized units called *banks*, allowing simultaneous access by threads within a warp. If multiple threads within a warp access the same bank with different words, the accesses are serialized, resulting in a phenomenon known as *bank conflict*.

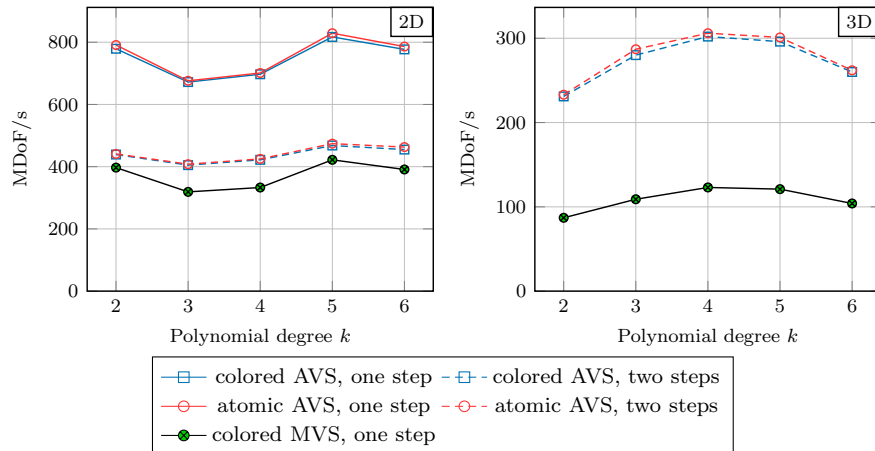


Figure 2: Throughput of the AVS and MVS smoothers with inexact local solver in two and three dimensions.

Figure 2 compares the performance of different smoother implementations measured in MDoF/s. It can be observed that atomic AVS achieves performance comparable to colored AVS, reaching up to 800 MDoF/s for a single smoothing operation in two dimensions. In contrast, the more complex MVS is significantly affected by the additional residual updates within each color, with performance dropping notably in three dimensions to 100 MDoF/s, approximately one-third of that of AVS. Overall, for different polynomial degrees, the shared memory computation model employed ensures stable performance in both two- and three-dimensional cases.

5.1 Numerical results

We present results on Cartesian grids in two and three dimensions with the coarse grid being the decomposition of the square or cube $[0, 1]^d$ into 2^d cells, consequently, it consists of one vertex patch. We use the multigrid V-cycle as a preconditioner in the conjugate gradient solver (CG) and in the generalized minimal residual method (GMRES) for the additive and multiplicative versions, respectively. The stopping criterion for the Krylov subspace methods is a relative residual reduction of 10^{-8} . On the coarse grid, we apply one smoothing step as the coarse grid solver. The right-hand side f is configured to yield an analytical solution of $u(x, y) = \sin(\pi x) \sin(\pi y)$ in two dimensions and $u(x, y, z) = \sin(\pi x) \sin(\pi y) \sin(\pi z)$ in three dimensions. We measure the efficiency of the preconditioners by reducing the Euclidean norm of the residual $\|r_n\|$ after n steps compared to the initial residual norm. Since the (integer) number of iteration steps depends strongly on the chosen stopping criterion, we

Table 1: Fractional iterations ν_{frac} for additive (AVS) and multiplicative (MVS) vertex patch smoothers in two dimensions, respectively with exact local solvers. CG/GMRES solver to relative accuracy 10^{-8} preconditioned by multigrid. Entries “—” not computed only levels L with 5×10^4 to 10^7 DoFs.

Level L	Convergence steps ν_{frac}					Colors
AVS	$k = 2$	$k = 3$	$k = 4$	$k = 5$	$k = 6$	
6	—	—	10.3	10.1	10.4	1
7	21.9	11.7	9.9	9.5	10.2	1
8	22.8	11.7	9.8	9.5	9.8	1
9	23.3	11.6	9.8	9.5	9.8	1
10	23.9	11.5	—	—	—	1
MVS	$k = 2$	$k = 3$	$k = 4$	$k = 5$	$k = 6$	
6	—	—	2.9	2.6	2.5	8
7	8.8	4.4	2.9	2.6	2.5	8
8	8.9	4.4	2.9	2.5	2.4	8
9	9.2	4.4	2.9	2.5	2.4	8
10	9.3	4.4	—	—	—	8

define the *fractional iteration count* ν_{frac} by

$$\nu = -8 \log_{10} \bar{r}, \quad \bar{r} = \left(\frac{\|r_n\|}{\|r_0\|} \right)^{1/n}.$$

First, we show the numerical efficiency of the vertex patch smoother in terms of iteration steps without taking any tensor structure into account. We perform two pre- and post-smoothing steps for the additive smoother with the natural relaxation parameter $\omega = 1/4$ and one pre- and post-smoothing step for the multiplicative smoother with the relaxation parameter $\omega = 1$. In Table 1 iteration counts for both the additive and multiplicative vertex patch smoother are compared. While both lead to uniform methods with respect to mesh level, the multiplicative method solves to high accuracy within 2–3 steps for polynomial degrees 4 and higher. Hence, they can be seen almost as direct solvers.

Comparing the number of solver iterations in Table 2 to those for exact local solvers in Table 1, we even observe a slight advantage for the inexact method in case of additive vertex patches. For low polynomial degrees k both multiplicative vertex patch methods compare at similar levels but with a growing gap in favor of exact local solvers if degrees increase: in particular, using inexact local solvers the number of iterations grows when increasing the polynomial degree while it decreases using exact local solvers. Nevertheless, the increase in iteration counts is moderate and absolute numbers are still low. The computational cost and memory intensity of these inexact but fast diagonalizable local solvers are significantly reduced, as reported in our previous work [CGBKS24]. There-

Table 2: Fractional iterations ν_{frac} for additive (AVS) and multiplicative (MVS) vertex patch smoothers in two dimensions, respectively with inexact local solvers. CG/GMRES solver with relative accuracy 10^{-8} preconditioned by multigrid. Entries “—” not computed only levels L with 5×10^4 to 10^7 DoFs.

Level L	Convergence steps ν_{frac}					Colors
	AVS	$k = 2$	$k = 3$	$k = 4$	$k = 5$	
6	—	—	9.2	9.9	10.3	1
7	19.2	10.4	9.0	9.3	9.8	1
8	19.6	10.3	9.0	9.2	9.5	1
9	19.9	10.3	9.0	9.1	9.4	1
10	20.1	10.2	—	—	—	1
MVS	$k = 2$	$k = 3$	$k = 4$	$k = 5$	$k = 6$	
6	—	—	4.2	4.5	5.2	8
7	9.2	4.8	4.2	4.5	5.2	8
8	9.4	4.8	4.2	4.5	5.1	8
9	9.5	4.8	4.2	4.4	4.9	8
10	9.5	4.8	—	—	—	8

fore, Schwarz smoothers with inexact solvers based on fast diagonalization are expected to be superior in computational efficiency.

In three dimensions, as shown in Table 3, while both the additive and multiplicative vertex patch smoothers yield methods that are uniform with respect to the mesh level, more iteration steps are required to achieve convergence compared to the two-dimensional case. This is because the inexact local solver in three dimensions becomes more inexact due to neglecting additional terms, as illustrated in (28). For AVP, a smaller relaxation parameter of $1/8$ is required in the three-dimensional case, though our experimental results indicate that a value of 0.1 provides better outcomes. For MVP, we use a damping factor of 0.7 , selected based on empirical experience. In general, MVP continues to outperform AVP, typically requiring around 10 iterations to converge, except for the case of $k = 6$.

5.2 Performance

The solver throughput plotted in Figure 3, measured as the number of unknowns solved per second, shows that the MVP is clearly superior to the AVP in two-dimensional case, especially for higher order elements. Since MVP requires fewer iterations, it demonstrates better performance in terms of solution efficiency, achieving more than 20 MDoF/s for polynomial degree $k = 6$. For AVP, introducing a second pre- and post-smoothing step significantly enhances performance by reducing the required number of iterations. In contrast, in three-dimensional cases, AVP shows better results. The increased number of colors

Table 3: Fractional iterations ν_{frac} for additive (AVS) and multiplicative (MVS) vertex patch smoothers in three dimensions, respectively with inexact local solvers. CG solver with relative accuracy 10^{-8} preconditioned by multigrid. Entries “—” not computed only levels L with 4×10^3 to 10^7 DoFs.

Level L	Convergence steps ν_{frac}					Colors
	AVS	$k = 2$	$k = 3$	$k = 4$	$k = 5$	
4	—	—	14.0	14.1	14.6	1
5	17.9	16.1	15.1	15.7	16.2	1
6	20.4	17.5	15.9	16.5	16.9	1
7	22.3	18.9	16.6	16.7	17.1	1
8	23.9	19.4	—	—	—	1
MVS	$k = 2$	$k = 3$	$k = 4$	$k = 5$	$k = 6$	
4	—	—	9.5	11.5	17.5	16
5	12.6	10.1	9.7	11.5	17.7	16
6	12.7	9.8	9.4	12.0	18.9	16
7	12.8	9.4	8.7	11.5	18.5	16
8	12.5	8.9	—	—	—	16

needed to restore parallelism in the MVP algorithm diminishes its advantage in convergence speed, as the additional residual update operations performed within each color outweigh its benefits.

In iterative or direct solutions of linear systems, introducing lower precision is often employed to accelerate computations, benefiting from its high performance number. However, using single precision throughout the entire solution process is typically insufficient to achieve acceptable accuracy and a mixed-precision approach combining an outer double-precision CG iteration with a single-precision multigrid V-cycle as a preconditioner demonstrated a same level accuracy and iteration count of a fully double-precision reference [GST07]. Additionally, a recent work [Cui24] shown that using half-precision computations with NVIDIA Tensor Cores achieved over a 4x speedup.

In our implementation, the preconditioner, specifically the multigrid V-cycle, is executed entirely in single precision, with data converted at the entry point of the V-cycle. Figure 4 compares the performance of a GMRES iteration run in double precision, preconditioned by a multigrid V-cycle with MVP for pre- and post-smoothing in single precision, against performing all computations in the V-cycle using double precision. For smaller problem sizes, both methods exhibit suboptimal performance as a result of insufficient parallelism to fully utilize the GPU. For larger problem sizes, we observed that the mixed-precision approach accelerated the solution of the linear system by 59% to 70%, capable of solving $8 \cdot 10^6$ unknowns per second in three dimensions.

In our final evaluation of the efficiency of the GPU implementation presented in this work, we compare the performance of the finite element operator and

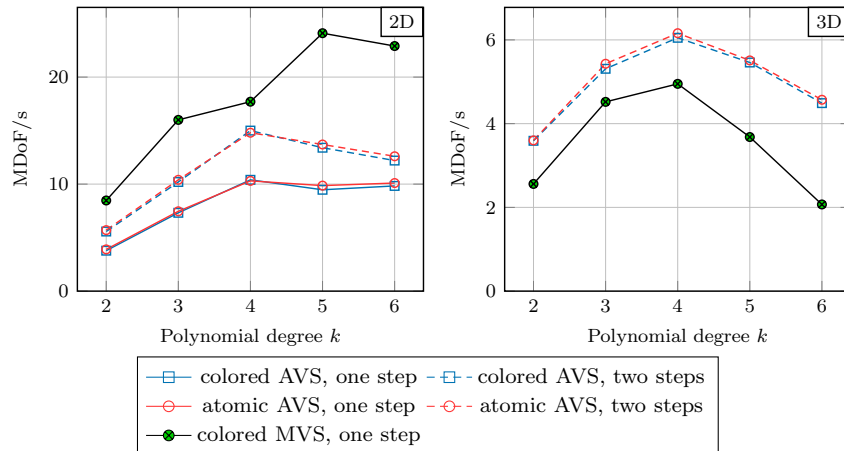


Figure 3: Throughput measured as the number of DoF solved per second for the AVS and MVS with inexact local solver in two and three dimensions. CG/GMRES solver with relative accuracy 10^{-8} preconditioned by multigrid.

the smoothing operator to that of the 3D Poisson problem, where the Poisson problem is discretized using the symmetric interior penalty method [CK24b]. We observed a 2–3x performance drop for the Biharmonic case to the Poisson problem. This is attributed to fact that the bilaplacian operator follows a rank-3 tensor representation (23), which involves additional terms, such as $L^{(1)} \otimes L^{(2)}$, compared to the laplacian operator. For the Poisson problem, the optimal performance is achieved at $k = 3$. This is because we use discontinuous Galerkin elements, which result in local operators and vector dimensions that are multiples of 8 ($= 2k + 2$), a configuration well-suited to GPU architectures.

We believe that the implementation can be further optimized by better aligning with GPU hardware characteristics. For example, zero-padding could be applied during data reads and operator computations to enhance cache utilization and thread efficiency. However, it is important to note that this approach increases shared memory consumption, particularly in three-dimensional cases. Therefore, a careful balance must be struck to avoid excessive shared memory usage that could reduce occupancy and degrade operator performance.

6 Conclusions

We have considered the C^0 -IP discretization of the biharmonic problem and we have presented exact vertex patch smoothers as well as an inexact version obtained by means of low rank tensor approximation. We have performed several numerical tests in two- and three-dimensional settings with the aim of showcasing the performances and demonstrating the efficiency of the proposed techniques. In particular, the approximation introduced by the low rank ap-

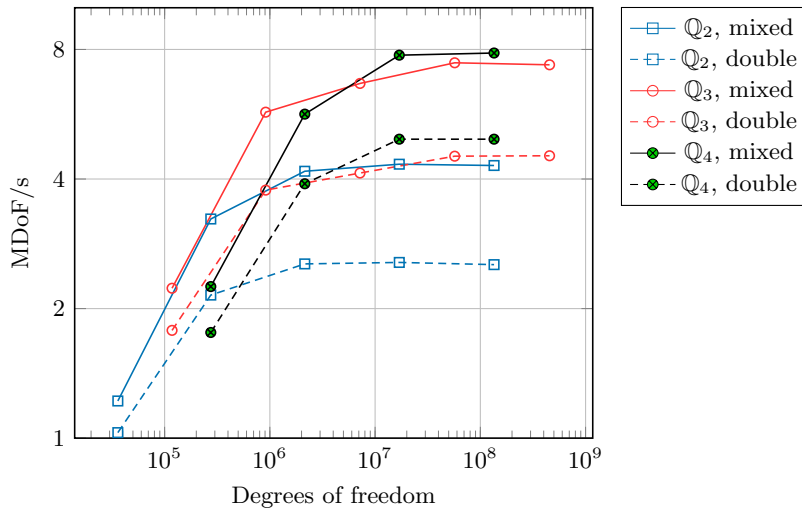


Figure 4: Comparison of double (solid) and mixed (dashed) precision performance for solving the biharmonic equation with GMRES preconditioned by multigrid with MVS with inexact local solver in three dimensions. Total solution time to relative accuracy 10^{-8} .

proximation still allows for a very fast converging multigrid methods with much less effort than the exact local solver. We observed that in the two-dimensional case the multiplicative smoother has shown superior performances, whereas in the three-dimensional case the additive smoother is shown to outperform its multiplicative counterpart. Moreover, the computations have been executed in mixed-precision: single precision for the multigrid preconditioner and double precision for the outer iteration of the multigrid preconditioner. The mixed precision method solves the problem almost twice as fast.

References

- [ABB⁺23] Daniel Arndt, Wolfgang Bangerth, Maximilian Bergbauer, Marco Feder, Marc Fehling, Johannes Heinz, Timo Heister, Luca Heltai, Martin Kronbichler, Matthias Maier, Peter Munch, Jean-Paul Pelteret, Bruno Turcksin, David Wells, and Stefano Zampini. The `deal.II` Library, Version 9.5. *Journal of Numerical Mathematics*, 31(3):231–246, 2023.
- [AFW97] Douglas N. Arnold, Richard S. Falk, and R. Winther. Preconditioning in $H(\text{div})$ and applications. *Mathematics of Computation*, 66(219):957–984, 1997.

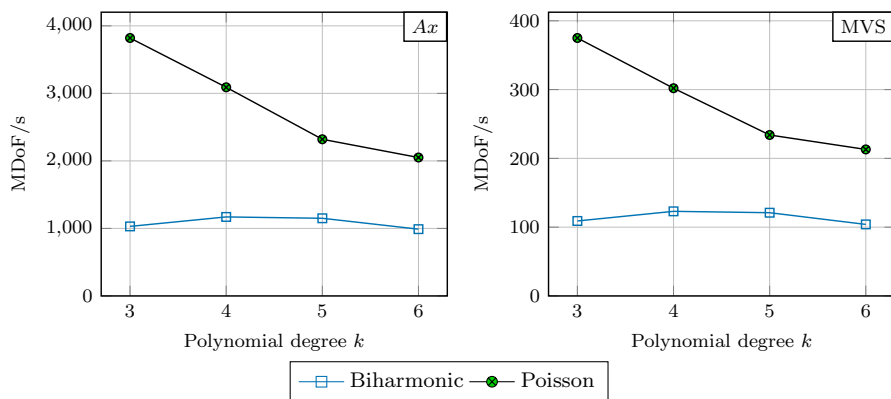


Figure 5: Comparison against Poisson problem for operator evaluation Ax and one MVS step with inexact local solver in three dimensions with same level of refinement, i.e. on 64^3 mesh.

- [Arn82] D. N. Arnold. An interior penalty finite element method with discontinuous elements. *SIAM J. Numer. Anal.*, 19(4):742–760, 1982.
- [Bre11] Susanne C. Brenner. C^0 interior penalty methods. In *Lecture Notes in Computational Science and Engineering*, pages 79–147. Springer Berlin Heidelberg, 2011.
- [BS05] Susanne C. Brenner and Li-Yeng Sung. C^0 interior penalty methods for fourth order elliptic boundary value problems on polygonal domains. *Journal of scientific computing*, 22-23(1-3):83–118, 2005.
- [BW05] Susanne C. Brenner and Kening Wang. Two-level additive Schwarz preconditioners for C^0 interior penalty methods. *Numerische Mathematik*, 102:231—255, 2005.
- [BZ05] Susanne C. Brenner and Jie Zhao. Convergence of multigrid algorithms for interior penalty methods. *Appl. Numer. Anal. Comput. Math.*, 2(1):3–18, 2005.
- [CGBKS24] Cu Cui, Paul Grosse-Bley, Guido Kanschat, and Robert Strzodka. An implementation of tensor product patch smoothers on GPU. *arXiv preprint arXiv:2405.19004*, 2024.
- [CK24a] Cu Cui and Guido Kanschat. Multigrid methods for the Stokes problem on GPU systems. *arXiv preprint arXiv:2410.09497*, 2024.
- [CK24b] Cu Cui and Guido Kanschat. Multilevel interior penalty methods on GPUs. *arXiv preprint arXiv:2405.18982*, 2024.

- [CPS18] D. Cho, L. F. Pavarino, and S. Scacchi. Isogeometric Schwarz preconditioners for the biharmonic problem. *Electron. Trans. Numer. Anal.*, 49:81–102, 2018.
- [Cui24] Cu Cui. Acceleration of Tensor-Product Operations with Tensor Cores. *ACM Trans. Parallel Comput.*, 11(4), 2024.
- [FK05] Xiaobing Feng and Ohannes A. Karakashian. Two-level non-overlapping Schwarz preconditioners for a discontinuous Galerkin approximation of the biharmonic equation. *J. Sci. Comput.*, 22(1–3):289–314, 2005.
- [GST07] Dominik GÖddeke, Robert Strzodka, and Stefan Turek. Performance and accuracy of hardware-oriented native-, emulated-and mixed-precision solvers in FEM simulations. *International Journal of Parallel, Emergent and Distributed Systems*, 22(4):221–256, 2007.
- [KK12] M. Kronbichler and K. Kormann. A generic interface for parallel cell-based finite element operator application. *Computers & Fluids*, 63:135–147, 2012.
- [KK19] Martin Kronbichler and Katharina Kormann. Fast matrix-free evaluation of discontinuous Galerkin finite element operators. *ACM Transactions on Mathematical Software (TOMS)*, 45(3):29, 2019.
- [KLM17] G. Kanschat, R. Lazarov, and Y. Mao. Geometric multigrid for Darcy and Brinkman models of flows in highly heterogeneous porous media: A numerical study. *Journal of Computational and Applied Mathematics*, 310:174–185, 2017.
- [KM15] G. Kanschat and Y. Mao. Multigrid methods for \mathbf{H}^{div} -conforming discontinuous Galerkin methods for the Stokes equations. *J. Numer. Math.*, 23(1):51–66, 2015.
- [KS14] Guido Kanschat and Natasha Sharma. Divergence-conforming discontinuous Galerkin methods and C^0 interior penalty methods. *SIAM J. Numer. Anal.*, 52(4):1822–1842, January 2014.
- [LRT64] Robert E. Lynch, John R. Rice, and Donald H. Thomas. Direct solution of partial difference equations by tensor product methods. *Numerische Mathematik*, 6(1):185–199, 1964.
- [MGS01] J.M. Melenk, K. Gerdes, and C. Schwab. Fully discrete hp-finite elements: fast quadrature. *Computer Methods in Applied Mechanics and Engineering*, 190(32–33):4339–4364, 2001.
- [Nit71] Joachim Nitsche. Über ein Variationsprinzip zur Lösung von Dirichlet-Problemen bei Verwendung von Teilräumen, die keinen Randbedingungen unterworfen sind. *Abhandlungen aus dem Mathematischen Seminar der Universität Hamburg*, 36(1):9–15, 1971.

- [NVI23] NVIDIA Corporation. Nsight Compute, 2023.
- [WMKK24] Michał Wichrowski, Peter Munch, Martin Kronbichler, and Guido Kanschat. Smoothers with localized residual computations for geometric multigrid methods. *arXiv preprint arXiv:2407.02100*, 2024.
- [Zha89] Shangyou Zhang. An optimal order multigrid method for biharmonic, C^1 finite element equations. *Numer. Math.*, 56:613–624, 1989.
- [Zha05] J. Zhao. Convergence of V- and F-cycle multigrid methods for the biharmonic problem using the Hsieh-Clough-Tocher element. *Numer. Methods PDE*, 21(3):451–471, 2005.